Synthesis and characterization of polyamide-6/graphite oxide nanocomposites

Yan Liu · Zhenming Chen · Guisheng Yang

Abstract Polyamide-6/graphite oxide (PA6/GO) nanocomposites were synthesized using delamination/absorption method. The morphologies of the composites were characterized by X-ray diffraction (XRD), scanning electron microscopy (SEM), and transmission electron microscopy (TEM). Both XRD and TEM showed that the GO sheets were completely exfoliated and distributed uniformly in PA6 matrix. Differential scanning calorimetry results revealed that the crystallization temperatures of the composites increased compared to that of pristine PA6, which was due to the heterogeneous nucleating effect of GO. However, the half-time of crystallization of the composites were evidently longer than that of pristine PA6, indicating an apparent decrease in the crystallization rate when GO was loaded into the polymer matrix. This was due to the constraining effect of layered GO on PA6 chains. The temperature of maximum decomposition rate was increased by 53 °C only by adding 5 wt% GO, and the maximum decomposition rate of the nanocomposites reduced greatly. The storage modulus (G') and loss modulus (G'') curves shifted to higher modulus upon addition of 1–5 wt% of GO. With increasing GO loading, the shear viscosity of the nanocomposites gradually increased compared with pure PA6.

Y. Liu · Z. Chen · G. Yang (✉)
Department of Polymer Science and Engineering,
Zhejiang University, Hangzhou, Zhejiang 310027,
People's Republic of China
e-mail: ygs@geniuscn.com

G. Yang
Shanghai Genius Advanced Materials Co., Ltd,
Shanghai 201109, People's Republic of China

Introduction

Nanocomposites attract a lot of attention from materials scientists because of their potentially novel properties. Their composition is such that they can be transformed into new materials possessing the advantages of the properties of both organic materials, such as light-weight, flexibility, and good moldability, and inorganic materials, such as high strength, heat stability, and chemical resistance. The incorporation of organic/inorganic hybrids results in materials possessing excellent stiffness, strength, and gas barrier properties [1]. In polymer clay nanocomposites, PA6/clay nanocomposites (PA6CN) exhibit 70% increase in modulus and strength. The heat distortion temperature increases from 65 °C of PA6 up to 150 °C of PA6CN, and the notched Izod impact strength of PA6CN is doubled at 5 wt% clay. These can be attributed to exfoliated layered structure of clay and strong interaction between clay layers and the PA matrix, which leads to some unique properties [2].

Graphite oxide (GO), also having the layered structure as that of clay, has attracted interest in the scientific community, especially in recent years [3–8]. GO, a representative pseudo-two-dimensional solid, by virtue of many functional groups attached on the layers, e.g., hydroxyl, carbonyl, and ether functional groups in the GO sheets, enables GO sheets to possess favorable microenvironment to form GO-intercalated or -exfoliated nanocomposites. Various polymer/GO composites, such as polyacrylated ester/GO [9], poly(ε-caprolactone)/GO [10], polystyrene/GO [11], poly(vinyl alcohol)/GO [12], poly(aniline-co-o-anisidine)/GO [13], poly(acrylic acid)/GO [14], polyethylene oxide/GO [15], have been prepared and characterized.

Polyamide-6 (PA6) is an important engineering plastic with excellent mechanical properties and good processability. However, it has a number of deficiencies, including

low thermal stability and poor dimensional stability. Numerous researches show that clays can play a pivotal role in improving the performance of polymers [16–20]. It is not surprising that GO can play the equivalent role as clays due to their similar layer microenvironment. It is expected that the incorporation of GO could endow PA6 with good electrical conductivity and thermal performance and further widen its potential application. However, few researches on the synthesis of PA6/GO composites with nano-dimension have been reported yet.

In this study, PA6/GO nanocomposites were prepared using delamination/absorption with dimethylacetamide (DMAC) as solvent. The morphologies, crystallization behavior, thermogravimetry, and rheological behaviors of PA6/GO nanocomposites were investigated.

Experimental part

Materials

Expandable graphite with a diameter of 80 mesh was supplied by Shandong New Fangyuan Industry Co., Ltd., (China). PA6 was obtained from Shanghai Genius Advanced Materials Co., Ltd., (China). It had an intrinsic viscosity of 0.94 dL/g in a sulfate acid/aqueous (96/4 wt/wt) solution at 25 °C. GO was prepared from expansible graphite by the modified Hummers method [21] and dried at 60 °C in a vacuum oven for 24 h.

Preparation of PA6/GO nanocomposite

PA6/GO nanocomposites were synthesized by delamination/absorption. 0.5 g GO was immersed in 100 mL DMAC and sonicated for 30 min to form delaminated suspension. The suspension was transferred quickly into a 500-mL three-necked round-bottom flask which was pre-placed in certain boiling DMAC solution of PA6. The flask was equipped with a mechanical stirrer. After stirring at a speed of 120 rpm for 3 min, the obtained mixture was poured into an empty beaker, cooled, filtered, and washed with acetone to remove DMAC. The resulting PA6/GO composite was dried at 60 °C for 24 h in a vacuum oven before characterization. Pristine PA6 was treated under the same procedure as for nanocomposites without adding GO. Corresponding to weight fractions of GO, the respective composites were designated as PA6-0 (0% GO), PA6-1 (1% GO), PA6-3 (3% GO), and PA6-5 (5% GO).

Characterizations

X-ray diffraction (XRD) analysis was performed using a Rigaku D/Max-III X-ray diffraction analyzer equipped with a rotating anode generator system using Cu Kα ($\lambda = 1.5406$ Å) radiation at an operating current of 200 mA with 2θ varying between 3° and 30°. The scanning speed was $1°$ min^{-1}, and the step size was 0.05°.

The morphology of pristine GO and the composites was characterized by a JSM-6700F field emission scanning electron microscope (FE-SEM) (Japan). Before SEM observation, the brittle fracture surfaces were coated with a thin layer of gold.

Transmission electronic microscopy (TEM) was carried out using a Hitachi H-800 microscope at an acceleration voltage of 100 kV. The nanocomposites were ultramicrotomed with a diamond knife on a Leica Ultracut UCT microtomed at room temperature to obtain nanometer-sized sections.

Differential scanning calorimetry (DSC) measurements were carried out using a NETZSCH DSC 200PC thermal analyzer. The dried PA6 and the nanocomposites were first heated at a rate of 60 °C/min from room temperature to 260 °C under nitrogen atmosphere, held for 5 min and then cooled to 50 °C at a cooling rate of 10 °C/min. The cooling processes were recorded.

Thermogravimetry was performed using a SDT Q600 (USA TA Instrument Corporation) at a heating rate of 20 °C/min from 50 °C to 700 °C under nitrogen flow.

The viscosity of pure PA6 and the nanocomposites were determined at 250 °C by ARES Rheometric Scientific rheometer with a parallel plate geometry (8-mm diameter and 1.0-mm gap width). The frequency was changed from 0.05 to 100 rad/s.

Results and discussion

XRD experiment

The X-ray powder diffraction (XRD) patterns of GO, PA6, and PA6/GO nanocomposites are presented in Fig. 1. The formation of an intercalated nanocomposite results in an increase in the d-spacing, while the formation of an exfoliated nanocomposite leads to the complete loss of registry between the layers [22]. It was observed from the above curves that there is a strong peak at $2\theta = 11.7°$ ($d_{001} = 7.55$ nm, according to Bragg equation $\lambda = 2d_{001}\sin\theta$) in the pattern of pristine GO, indicating an interspacing of 7.55 nm. However, the pattern of PA6/GO composites only exhibits two characteristic diffraction peaks of PA6, at $2\theta = 19.8°$ and $2\theta = 23.7°$. The strong diffraction peak of GO in the composite disappears, which demonstrates that the GO layers are stripped into a single layer structure and they are completely exfoliated in the composite. This will be further proven in the subsequent TEM research.
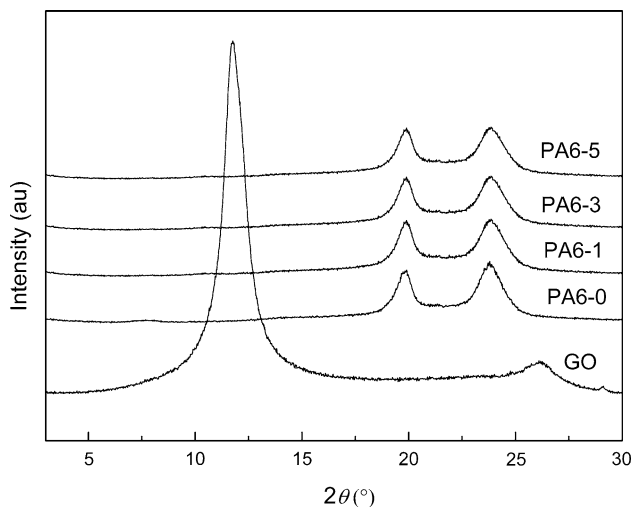
Fig. 1 XRD patterns of GO, PA6, and the PA6/GO nanocomposites

SEM observation

The scanning electron microscopy (SEM) images of pristine GO (a and b) and PA6-5 nanocomposite (c and d) are shown in Fig. 2. From Fig. 2a, we can see the layer-like GO with a size of about 200 μm piling up over each other. The fringe of the GO curls as indicated by the ellipse. Fig. 2b gives a more clear observation of the GO fringe. The GO fringe shows many strata-like loosely stacked

layers, which makes it easier for PA6 chains to insert the pores of GO and exfoliate the sheets. Figure 2c and d present the morphologies of PA6-5 composite. It is clear that the morphology of the PA6/GO composite is different from that of GO. GO sheets in the composite have been completely exfoliated. The thickness of the sheet is in the range of several to dozens of nm. Many PA6 fibers can be found on the edges of the GO sheets, confirming the excellent compatibility and the strong interaction between the sheets of GO and PA6 matrix, which can be attributed to the synergic effects of function groups between GO sheets and PA6 chains.

TEM observation

The TEM images of the PA6/GO composite are shown in Fig. 3. Figure 3a and b shows that the interspacing between two neighbor dark lines is increased to 50–80 nm, which indicates that PA6 chains has been inserted to the sheets of GO. In addition, the exfoliated GO shows large aspect ratio. For PA6-3 and PA6-5, most of the GO sheets (disordered dark lines), with a layer thickness of 10–20 nm, dispersed well in the PA6 matrix, which is consistent with the results of XRD and SEM. In addition, the fine dispersion and large aspect ratio of the GO sheets in the composite will lead to a remarkable improvement on the properties of PA6, especially in regard to mechanical properties.
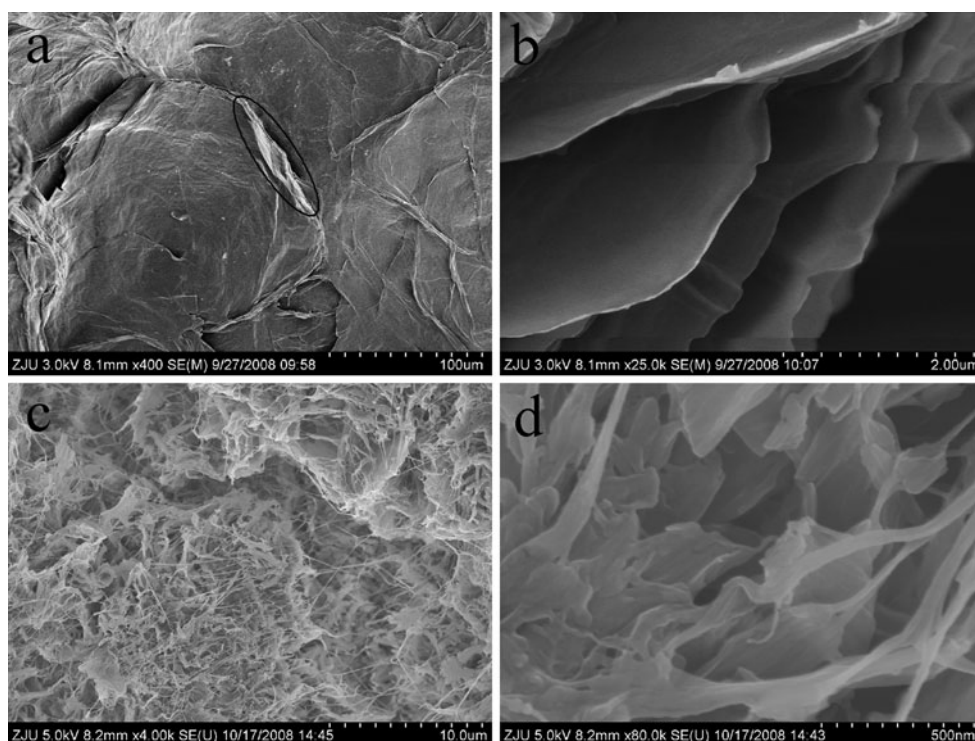

Fig. 2 Scanning electron microscopy of **a** GO, **c** PA6-5 nanocomposite, **b**, **d** are magnification of **a**, **c**, respectively
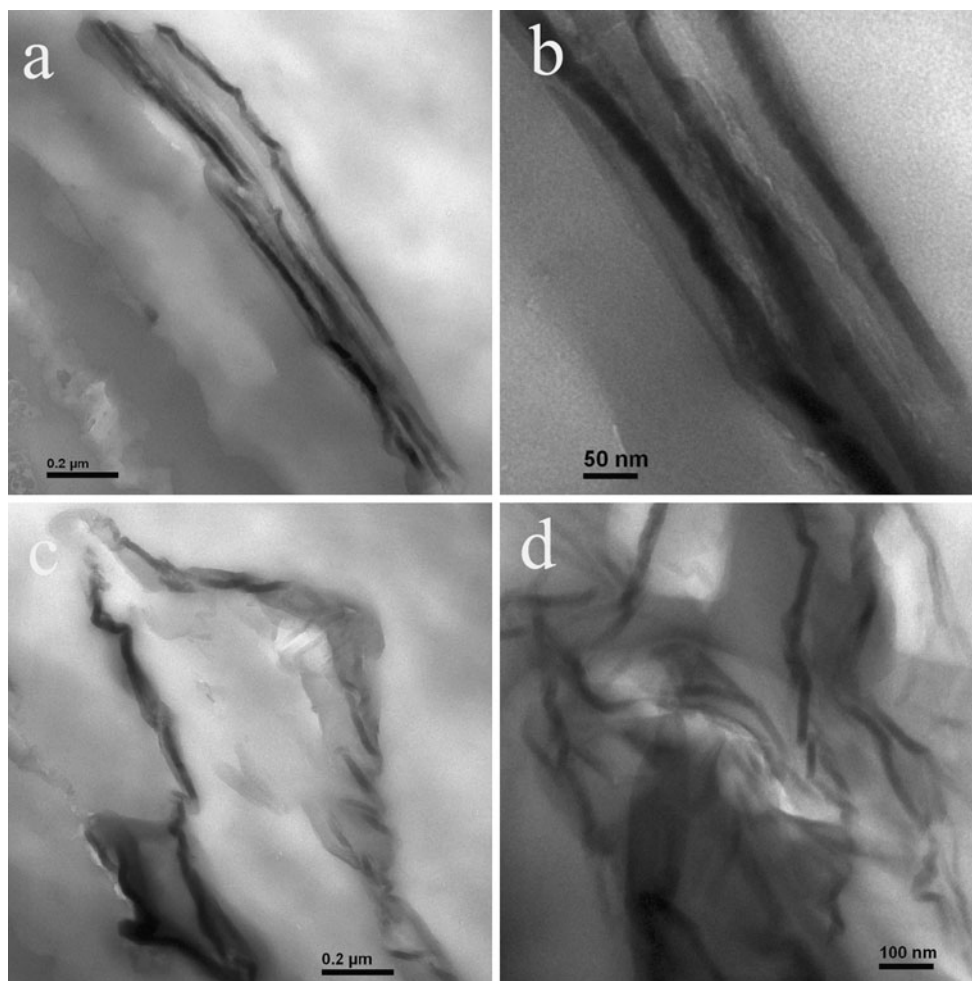
Fig. 3 Transmission electron micrographs of **a** PA6-1, **c** PA6-3, and **d** PA6-5 nanocomposites. **b** is a magnification of **a**

Crystallization behaviors

The melt-crystallization behaviors of PA6 and PA6/GO nanocomposites are shown in Fig. 4. The DSC parameters of cooling process are summarized in Table 1. As shown in Fig. 4 and Table 1, the crystallization exothermal peaks of the composites all shift to high temperature compared to neat PA6, which suggests that GO, act as heterogeneous nucleating agent, increases the melt-crystallization temperature (T_c). Moreover, the greater the content of GO, the higher the T_c. Comparing the crystallization enthalpy (ΔH_c) of the composites with that of pristine PA6, we find that the composites exhibit higher values, and this implies that the crystallinity degrees of the composites are increased.

By a careful observation, we find that the PA6/GO composite shows widening crystallization exotherm compared with pristine PA6, which indicates a long crystallization time. The half-time of crystallization ($t_{1/2}$) is a parameter which can be used to evaluate the crystallization rate of polymer. It is defined as the time taken from the
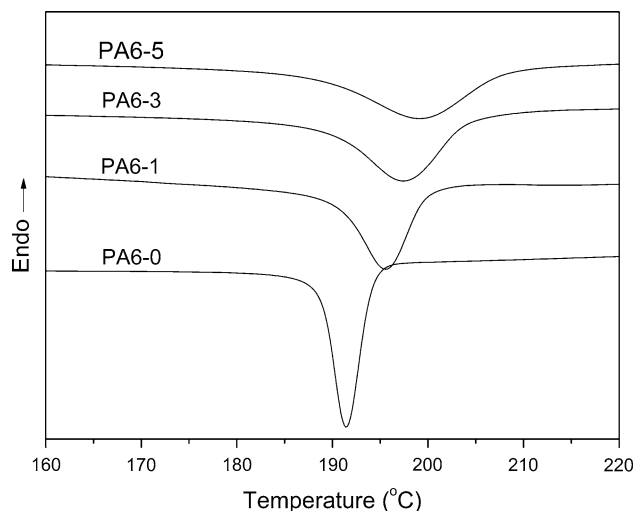

Fig. 4 DSC curves of PA6 and PA6/GO nanocomposite

onset of $X_c(t)$ until 50% completion. In general, the smaller the value of $t_{1/2}$, the faster the crystallization rate. From Table 1, we can see that the $t_{1/2}$ of the composite is
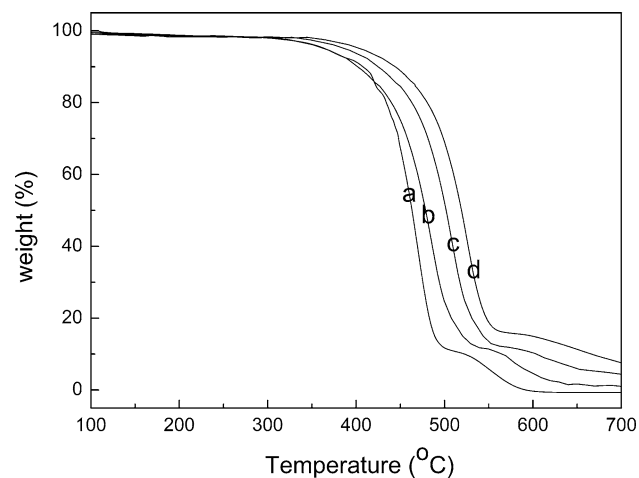
Table 1 DSC parameters of melt-crystallization for PA6 and PA6/GO composites

Samples	T_c (°C)	ΔH_c (J/g)	$t_{1/2}$ (s)
PA6-0	191.4	54.7	34.3
PA6-1	195.7	55.4	39.1
PA6-3	197.4	56.6	61.4
PA6-5	199.4	57.9	82.0

evidently longer than that of pristine PA6, and this suggests an apparent decrease in the crystallization rate when GO is loaded into the polymer matrix.

Actually, GO has dual effects in the matrix. First, GO can accelerate crystallization by providing added surface nucleation sites, a positive effect on crystallization. Second, the GO sheets (as seen in Fig. 3) can also constrain the crystallization rate because the exfoliated sheets hinder the migration and diffusion of PA6 chains to the surface of the nucleus, and they constrain spherulite growth, a negative effect on crystallization [23, 24]. At high GO loading, the constraining effect plays a predominant role. The positive effect is relatively feeble. Therefore, the composites exhibit slower crystallization rate than that of pristine PA6.

According to the literature [25], PA6 exhibits a relatively rapid crystallization rate, which results in some

Fig. 5 TGA curves in nitrogen at the heating rate of 20 °C/min for (*a*) PA6-0, (*b*) PA6-1, (*c*) PA6-3, and (*d*) PA6-5

drawbacks such as high mold shrinkage and dimensional instability. Therefore, GO may be an ideal agent for PA6 processing.

Thermal stability

The effect of GO on thermal stability of PA6 matrix was investigated. Typical TGA for PA6 and the nanocomposites are shown in Fig. 5. PA6 and PA6/GO nanocomposites show similar degradable process. That is, both PA6 and the nanocomposites exhibit two main degradation stages. The decomposing temperature, at which the weight loss of the sample is 50% ($T_{50\%}$), the maximum decomposing rate temperatures (T_{max1} and T_{max2}), the maximum decomposing rate (R_{max}), and the residues at 450 and 700 °C are presented in Table 2. As seen in Table 2, the values of $T_{50\%}$ of the composites are much higher than that of pristine PA6. T_{max1} of PA6 and the composite are 469.9, 485.0, 508.8, and 523.0 °C. The maximum improvement is 53 °C for the composite which contains 5 wt% GO. T_{max2} of the composite also shows a diminutive peak compared with that of pristine PA6. In addition, the R_{max} is also reduced from 1.67 to 1.55, 1.46, and 1.35 for PA6-0, PA6-1, PA6-3, and PA6-5, respectively. It has been found that the main route of thermal degradation of PA6 is the formation of caprolactam with yields as high as 85% [26, 27]. The residual weight fractions of PA6-0, PA6-1, PA6-3, and PA6-5 at 450 °C are 67.2, 75.2, 84.8, and 89.2 wt%, respectively. At 700 °C, pristine PA6 almost degraded completely, while the composite has certain residue. These results indicate that the GO could improve the thermal stability of matrix, because of the fine dispersion and barrier effect of GO sheets in the composite, and thus postpone the degradation of the matrix [28]. The residual weight of the composite at 700 °C is higher than the theoretical amount of GO present in the hybrid materials. This can be explained by the fact that some organic chains may remain trapped inside the inorganic network giving a higher residue at a higher temperature [29].

Rheological behavior

Figure 6a, b shows the storage modulus (G') and loss modulus (G'') of neat PA6 and the composites measured

Table 2 The kinetic parameters of TGA for PA6 and PA6/GO composite

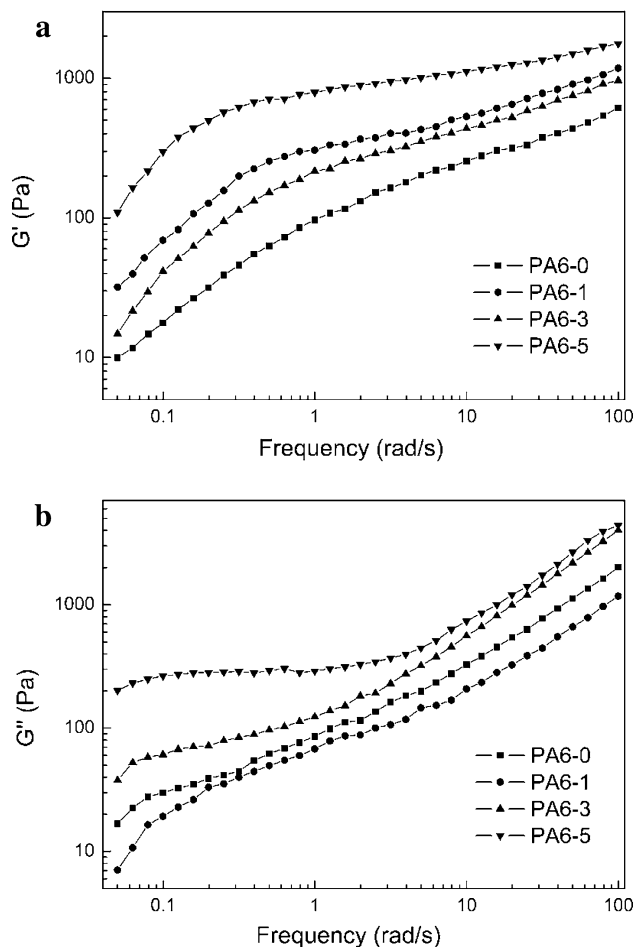| Samples	$T_{50\%}$ (°C)	T_{max1} (°C)	T_{max2} (°C)	$R_{max}\%$ (°C)$^{-1}$	Residue at 450 °C (wt%)	Residue at 700 °C (wt%)
PA6-0	463.2	469.9	553.3	−1.67	67.2	0.02
PA6-1	478.3	485.0	577.0	−1.55	75.2	1.3
PA6-3	501.0	508.8	623.0	−1.46	84.8	4.4
PA6-5	524.6	523.0	650.0	−1.35	89.2	7.8

Fig. 6 **a** Storage modulus, **b** loss modulus as a function of frequency for neat PA6 and the composites of varying GO content at 250 °C

Fig. 7 Steady-state shear viscosity as a function of frequency for pure PA6 and the nanocomposites

over a frequency range of 0.05–100 rad/s at 250 °C. It is apparent that both storage and loss modulus increase monotonically with increasing frequency for PA6 and the composites. Moreover, both the G' and G'' curves shift to higher modulus upon addition of 1–5 wt% of GO. The G' and G'' represent the stiffness and the viscous response of the material, respectively [30]. A higher frequency in the dynamic mechanical analysis means a higher loading rate. A higher loading rate has been found to cause a higher elastic modulus [31]. As shown in Fig. 6a and b, the GO has a significant reinforcing effect on the G' and G'', especially at low frequencies and high GO loading.

By a careful observation, we find that, at high content of GO (i.e., 5 wt%), both G' and G'' begin to level off and exhibit a plateau at a low value of frequency. This is in agreement with previous results [32–34]. When the GO concentration value increases, GO–GO interactions begin to dominate, leading to percolation and the formation of an interconnected structure of GO (Fig. 3d). The appearance of a plateau at low value of frequency is understood to be the result of agglomeration of fillers.
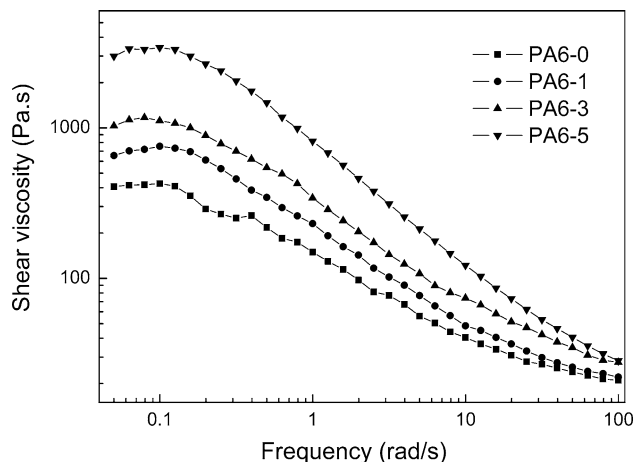
The steady-state shear viscosity of neat PA6 and nano-composites as a function of frequency is shown in Fig. 7. Apparently, all the composites exhibit pseudoplastic behavior, i.e., the viscosity decreasing disproportionately with increasing frequency. The composites reveal higher shear viscosity than pure PA6. Moreover, the greater the content of GO, the higher the shear viscosity. The enhancement in the shear viscosity due to the presence of rigid fillers in dilute suspensions had been proposed by Einstein [35] who pointed out that the enhancement in the shear viscosity was a result of increased energy dissipation attributable to the presence of the particles. In more concentrated suspensions, stronger interactions between filler and matrix give rise to much larger energy dissipation, resulting in an appreciable increase in the shear viscosity.

Conclusion

PA6/GO composites with nanoscale-dispersed GO sheets were successfully prepared by delamination/absorption, and they were evaluated through SEM, TEM, DSC, TGA, and rheometer. Both XRD and TEM showed that the GO sheets were completely exfoliated and distributed uniformly in PA6 matrix. The crystallization temperatures of all the composites were higher than that of pristine PA6, which indicated that GO, acting as heterogeneous nucleating agent, increased the T_c of PA6. However, the half-time of crystallization of the composite was evidently longer than that of pristine PA6, indicating an apparent decrease in the crystallization rate when GO was loaded into the polymer matrix. This was because the exfoliated layers of GO hinder the migration and diffusion of PA6 chains to the surface of the nucleus, and they constrain spherulite growth. TGA result showed that the composites show much higher

thermal stability than PA6, and the temperature of maximum decomposition rate was increased by 53 °C only by adding 5 wt% GO. In addition, the maximum decomposition rate of the nanocomposites reduced greatly.

Both the storage modulus (G') and loss modulus (G'') increased monotonically with increasing frequency for PA6 and the composites. G' and G'' all shifted to higher modulus upon addition of 1–5 wt% of GO. PA6 and the nanocomposites investigated in this study exhibited the expected shear-thinning behavior. With increasing GO loading, the shear viscosity of the nanocomposites gradually increased compared with pure PA6 at a given frequency.

References

1. Chang JH, Kim SJ, Joo YL, Im S (2004) Polymer 45:919
2. Clifford MJ, Wan T (2010) Polymer 51:535
3. Szabó T, Tombácz E, Illés E, Dékány I (2006) Carbon 44:537
4. Szabó T, Szeri A, Dékány I (2005) Carbon 43:87
5. Matsuo Y, Tabata T, Fukunaga T, Fukutsuka T, Sugie Y (2005) Carbon 43:2875
6. Cerezo FT, Preston CML, Shanks RA (2007) Compos Sci Technol 67:79
7. Zhang R, Hu Y, Xu J, Fan W, Chen Z (2004) Polym Degrad Stab 85:583
8. Kaczmarek H, Podgórski A (2007) Polym Degrad Stab 92:939
9. Wang JQ, Han ZD (2006) Polym Adv Technol 17:335
10. Kai WH, Hirota Y, Hua L, Inoue Y (2008) J Appl Polym Sci 107:1395
11. Uhl FM, Wilkie CA (2004) Polym Degrad Stab 84:215
12. Xu JY, Hu Y, Song L, Wang QG, Fan WC, Liao GX (2001) Polym Degrad Stab 73:29
13. Wang GC, Yang ZY, Li XW, Li CZ (2005) Carbon 43:2564
14. Xu JY, Hu Y, Song L, Wang QG, Fan WC (2002) Carbon 40:2961
15. Matsuo Y, Tahara K, Sugie Y (1997) Carbon 35:113
16. Manias E, Touny A, Wu L (2001) Chem Mater 13:3516
17. Bourbigot S, Devaux E, Flambard X (2002) Polym Degrad Stab 75:397
18. Giannelis EP (1996) Adv Mater 8:29
19. Messoria M, Tosellib M, Pilatia F (2003) Polymer 44:4463
20. Zheng X, Wilkie CA (2003) Polym Degrad Stab 81:539
21. Hummers WS, Offeman RE (1958) J Am Chem Soc 80:1339
22. Zhu J, Morgan AB, Wilkie CA (2001) Chem Mater 13:3774
23. Run MT, Yao CG, Wang YJ, Song HZ (2008) Polym Compos 29:1235
24. Yao CG, Yang GS (2009) Polym Adv Technol 20:768
25. Brandrup J, Immergut EH, Grulke EA (1997) Polymer handbook, 4th edn. Chapter 6, Solid state properties. Wiley, New York, p 279
26. Levchik SV, Costa L, Camino G (1992) Polym Degrad Stab 36:229
27. Czernik S, Elam CC, Evans RJ, Meglen RR, Moens L, Tatsumoto K (1998) J Anal Appl Pyrol 46:51
28. Liu AD, Xie TX, Yang GS (2006) Macromol Chem Phys 207:1174
29. Ding RF, Hua Y, Gui Z, Zong RW, Chen ZY, Fan WC (2003) Polym Degrad Stab 81:473
30. Zhang YF, Bai SL, Yang DY, Zhang Z, Walter SK (2008) J Polym Sci Part B: Polym Phys 46:281
31. Fang TH, Chang WJ (2004) Microelectron J 35:595
32. Lakadawala K, Salovey R (1987) Polym Eng Sci 27:1035
33. Lakadawala K, Salovey R (1988) Polym Eng Sci 28:877
34. Wu G, Zheng Q (2004) J Polym Sci Part B Polym Phys 42:1199
35. Einstein A (1911) Ann Phys 34:591